

Final report

**Benchmarking of Absolute and Relative
Positioning Solutions under GNSS Denied
Environments for Mobile Geomatics**

ISPRS Scientific initiative 2023

Principal Investigators

Yunsheng Wang¹ and Liang Chen²

Co-investigators

Haiyun Yao², Xiaochen Wang², Hanwen Qi², Teemu Hakala¹, Jesse Muhojoki¹, J. Wang³ and Zhengjun Liu⁴

¹Finnish Geospatial Research Institute, Finland; ²Wuhan University, China; ³China University of Mining and Technology, China; ⁴Chinese Academy of Surveying and Mapping, China.



1. Project objectives

The project aims to evaluate the performance of absolute and relative positioning solutions in GNSS denied environments through an international benchmarking with comparison to ground truth data measured by conventional methods. We focused on assisting reliable quantitative benchmarks about the positioning accuracies and stabilities of the compared solutions. A comprehensive benchmarking was carried out in this study based on the comparisons of six solutions that consist of different combinations of five positioning technologies, i.e., 1) ultra-wideband (UWB) and inertial measurement unit (IMU); 2) UWB, IMU, and camera; 3) UWB and light detection and ranging (LIDAR); 4) UWB and radio detection and ranging (RADAR); 5) IMU, camera and LIDAR; and 6) UWB, IMU, camera and LIDAR.

Main objectives:

- To quantitatively analyze and evaluate the performance of the hybrid positioning system (HPS) by using high-quality survey-level reference, which is current absent in most studies.
- To develop new algorithms for precision positioning, such as the UWB anchor self-positioning algorithm that simultaneously estimates the positions of UWB anchors and tracks UWB tag in real-time, and the integrity monitoring (IM) algorithm that mitigates the adverse NLOS impacts.
- To reveal the strengths and limitations of individual positioning solution and their combinations.
- To evaluate the potentials of HPS systems through quantitative comparison under GNSS denied/challenged environments.

2. Datasets

2.1 Platform and Sensors

The equipment used in the experiment is shown in Fig. 1. The mobile platform was the SCOUT mini model UGV (AgileX Robotics, Shenzhen, China). The positioning sensors included a set of LinkTrack P-B UWB devices (NoopLoop Technology Co., Ltd, Shenzhen, China), a RealSense Tracking Camera T265 (Intel, California, USA), a PandarXT-32 laser LiDAR (Hesai Technology, Shanghai, China), an Eagle mmWave RADAR (Oculii, Ohio, USA). The onboard computing unit was an Intel NUC computer (Intel, California, USA).

The LiDAR had a 0.5-centimeter (cm) ranging accuracy, a 120-meter measuring range, a 360°/31° horizontal/elevational field of view (FOV), and a 0.18° horizontal angular resolution, and a 10 Hz scan rate at 32 lines/sec. The RADAR had a 0.86 meter (m) ranging accuracy, a 400-meter measuring range, a 120°/45° horizontal/elevational field of view (FOV), < 1° horizontal angular resolution, and a 15 Hz scan rate. The UWB had a tag and four anchors. The T265 camera includes two fisheye lens sensors with a combined 163° FOV (+/- 5°). The UWB tags and T265 camera all have low-cost MEMS-IMU. The UWB tag has MPU-6500 (InvenSense Company, California, USA), and the T265 has BMI055 (BOSCH Company,

Stuttgart, Germany).

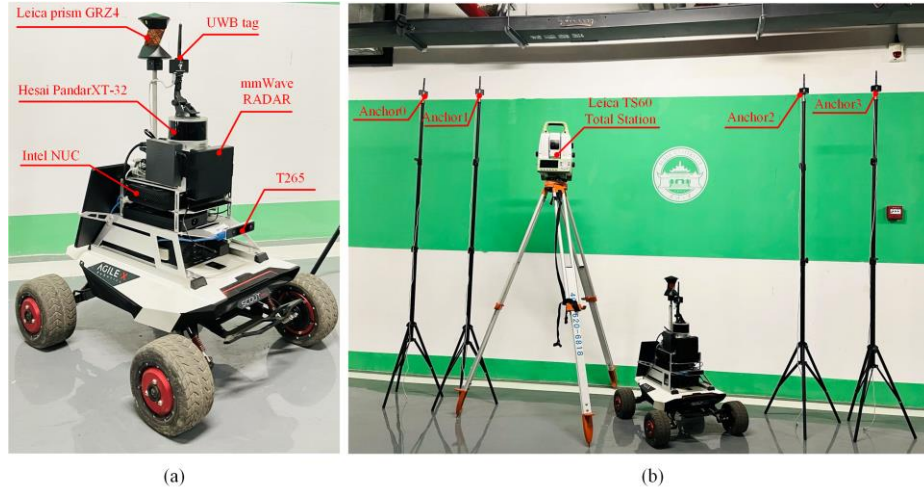


Fig. 1. The experiment equipment (a) The multi-sensors positioning platform; (b) The total station and UWB anchors

2.2 Experiment Setup

The performances of the absolute and relative positioning solutions were evaluated and compared in four indoor and outdoor experimental scenes in this paper. In each experiment, a roughly repeated route was gone through three times. Single and repeated routes were compared, to evaluate the drifting effects over time of the relative positioning, i.e., IMU, camera, LIDAR, and RADAR.

Table 1 summarized experimental scenes and their ground truth. The experiments were numbered according to the site and trajectory number. For instance, the experiments in the indoor meeting room with single and repeated trajectories were named Indoor I-1 and I-3, respectively.





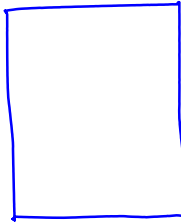
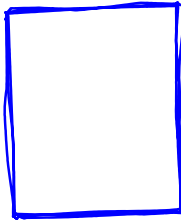


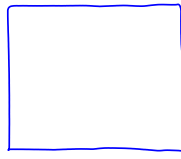
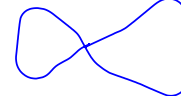
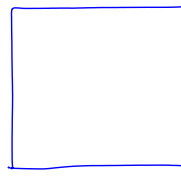
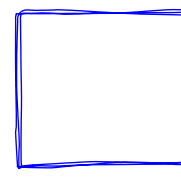
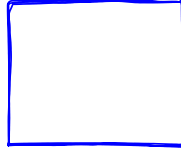

2.3 Reference Data

The reference trajectories, or the ground truths, were collected using a Leica TS60 total station and a GRZ4 360°prism (Leica, Heerbrugg, Switzerland) fixed on the UGV. The GRZ4 360° prism delivers an overall accuracy of 2-5 millimeters and an automatic target recognition of up to 600 meters.

2.4 UWB sensor networks

In absolute positioning, the positioning accuracy is affected by both the algorithm and geometry of UWB sensor networks, similar to the satellite constellation. The dilution of precision (DOP), an indicator of satellite geometry for the satellite constellation, was used to evaluate the network configuration. The two-dimensional plane positioning accuracy within the UWB networks was simulated to reveal the impacts of the geometry of UWB networks, i.e., the Horizontal Dilution of Precision (HDOP). A smaller HDOP value represents a more optimal geometry of sensor networks for positioning.

Table 1. Experiment sites and setup

	Indoor				Outdoor					
Sites	Meeting Room		Underground Parking		Library Square				Basketball Court	
Snapshot										
Description	Many tables and chairs. With some NLOS.		Relatively empty.		Empty, surrounding objects, e.g. walls, trees., etc.				Empty, objects on one side.	
Notation ^a	Indoor I-1	Indoor I-3	Indoor II-1	Indoor II-3	Outdoor I		Outdoor II		Outdoor III-1	Outdoor III-3
Size of tested area (m ²)	10×10		13×7		17×17				15×15	
The lengths of the Ground Truth (m)	28.4	84.8	28.3	83.7	Outdoor I-1	52.4	Outdoor II-1	51.8	46.3	139.4
					Outdoor I-3	156.2	Outdoor II-3	155.5		
Ground truth trajectories					Outdoor I -1		Outdoor II -1			
					Outdoor I -3		Outdoor II -3			

^a The letter “I, II, III” denotes the site numbers; Numbers “1” and “3” mean the site was covered by 1 and 3 trajectories, respectively.

3. Algorithms and Solutions in the Benchmarking

This project assembled the six hybrid positioning systems (HPSs) to fully test the positioning performance of five absolute and relative positioning sensors in GNSS denied environment. Moreover, different methods for the fusion of sensors in each HPS solution were also studied. The details of six benchmarked HPS solutions, including the fusion engines, positioning algorithms, and integrity monitoring, were summarized in the Table 2.

Table 2. The detailed information of the six HPSs

HPSs		Fusion Engines	Relative Positioning Algorithms	Integrity Monitoring
1	UWB-IMU	EKF-LC	SINS	IBIM
		UKF-LC		PROD, IBIM
		EKF-TC		
		UKF-TC		
2	UWB-CAMERA-IMU	EKF-TC	ORB-SLAM3	PROD, IBIM
3	UWB-LiDAR		A-LOAM	
4	UWB-RADAR			
5	IMU-CAMERA-LiDAR	EKF-LC	SINS, ORB-SLAM3, A-LOAM	IBIM
6	UWB-IMU-CAMERA-LiDAR	EKF-STC		PROD, IBIM

HPS-1 integrates UWB and IMU, and four fusion methods, i.e., EKF-LC, EKF-TC, UKF-LC, and UKF-TC, were compared to analyze their performances. The UKF fusion algorithm was tested only in HPS-1 because the state models of HPS-2, -3, and -4 and the measurement model of HPS-5 are linear. The integration between UWB and CAMERA in HPS-2, and HPS-3, as well as between LIDAR and RADAR in HPS-4 are carried out using EKF-TC, to study the performances of different combinations of the relative and absolute positioning. HPS-5 evaluated only the relative positioning performance, i.e., IMU, CAMERA, and LIDAR, based on EKF-LC. HPS-6 tested the performance of multiple positioning subsystems based on STC, i.e., when UWB, IMU, CAMERA, and LIDAR are all combined. In the experiments, the strap-down inertial navigation system (SINS) used IMU positioning, the ORB-SLAM3 algorithm in a stereo-inertial mode used CAMERA positioning, and the A-LOAM algorithm was used for LIDAR and RADAR positioning.

HPS-1 included both TC and LC, where TC is illustrated in Fig 2. The pseudo ranges between the UWB anchors and tag were based on the time of flight (TOF). The outliers of pseudo ranges affected by NLOS were eliminated in the IM, and the filtered pseudo ranges were input into the fusion engine. The anchor positions were estimated by the proposed UWB anchor self-positioning algorithm in real-time (see Section IV.E). In the IMU positioning subsystem, the real-time position, velocity, and attitude (PVA) were obtained by the SINS algorithm given initial IMU PVA, acceleration, and gyroscope zero bias. The ranges between the anchors and IMU can be estimated using anchor and IMU positions in real-time.

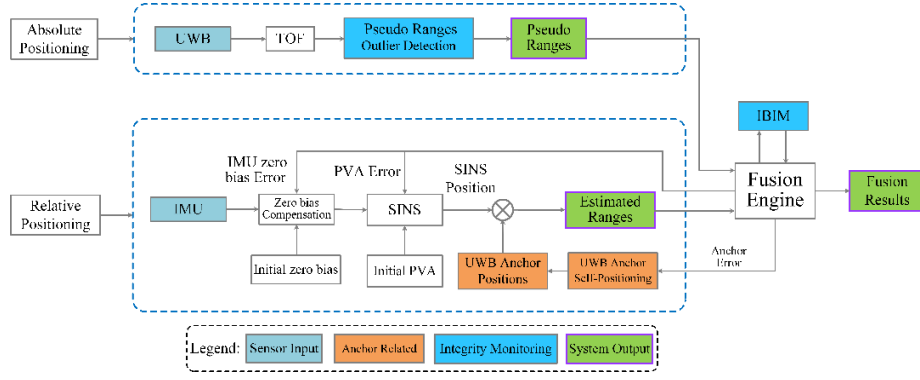


Fig. 2. Block diagram of the HPS-1 based on the tightly couple.

HPS-2, -3, and -4 integrated the absolute positioning subsystem UWB and the relative positioning subsystem camera-IMU, LIDAR, and RADAR, respectively. The system error state model refers to the distance error between UWB anchors and the tag. The system measurement model refers to the difference between the estimated ranges inferred by the relative position subsystem and pseudo ranges calculated by the absolute position subsystem. The optimal state estimate after filtering would feedback to the estimated range between the UWB anchors and relative positioning sensors (i.e., CAMERA, LIDAR, and RADAR) as illustrated in Fig. 3. The corrected range estimation was used to solve the final position information by the least square.

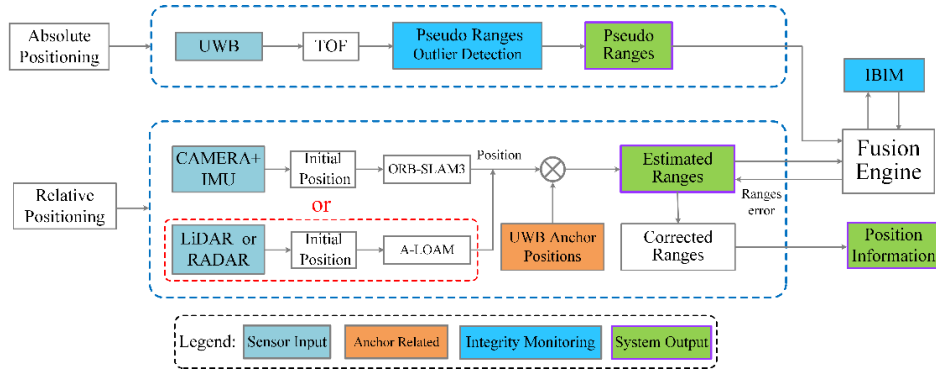


Fig. 3. Block diagram of the HPS-2 (UWB+CAMERA+IMU), HPS-3 (UWB+LiDAR), and HPS-4 (UWB+RADAR) based on tight coupling.

HPS-5 combined three relative positioning sensors, i.e., IMU, CAMERA, and LIDAR, as illustrated in Fig. 4. The system state model was the same as that of HPS-1. The system measurement model referred to the difference between CAMERA and IMU positions, and the LIDAR and IMU positions. The proposed IBIM was performed to improve the accuracy as well as the robustness of the positioning system. The real-time estimated state vector errors were feedbacked to the SINS and the fusion results were obtained through the error feedback correction.

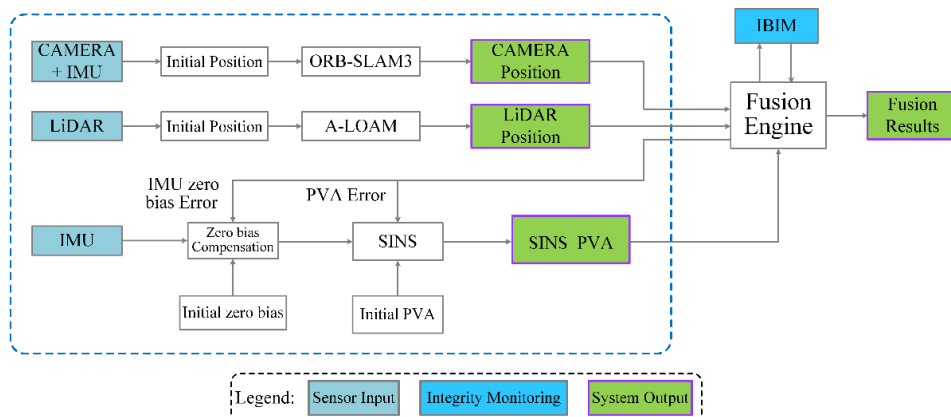


Fig. 4. Block diagram of the HPS-5 based on the loose coupling.

HPS-6 combined all absolute and relative positioning sensors as illustrated in Fig. 5. HPS-6 added two relative positioning of CAMERA and LIDAR in addition to HPS-1. To compensate for the shortcomings of the tight and loose coupling, the fusion engine adopts a semi-tight couple method. In the fusion engine, the system state model was the same as that of HPS-1. The system measurement model was divided into two parts. The first part was the difference between the estimated range from the UWB anchors positions to the IMU position and pseudo ranges calculated by the absolute position subsystem. The second part was the difference between the position of the camera and the position of the IMU and the position difference between the position of the LIDAR and the IMU. The proposed integrity monitoring detects outliers in real-time. The real-time estimated state vector errors were feedbacked to the SINS and the fusion results will be obtained through the error feedback correction.

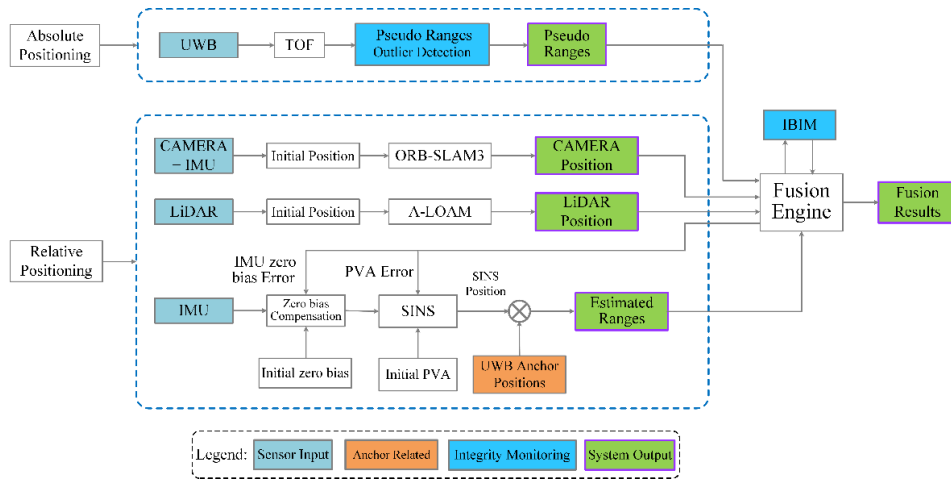


Fig. 5. Block diagram of the HPS-6 based on the semi-tight coupling.

4. Results

The six proposed HPSs were tested in four indoor and outdoor experimental scenes to benchmark the absolute and relative positioning in both single and repeated trajectories. Further, the experiments also evaluated the performance of the fusion methods with different sensor combinations.

4.1 Indoor Scenarios

Extensive experiments were carried out to validate the six HPSs in two indoor experimental scenarios. The positioning methods of the UWB, the CAMERA+IMU, and the LIDAR were the multilateration, the ORB-SLAM3, and the A-LOAM, respectively. The mmWave RADAR was conducted only in underground parking (Indoor-II) scenes because of the sensor availability.

For Indoor-I, the cumulative distribution function (CDFs) of error corresponding to the different HPSs are shown in Fig. 6 and the error statistics are shown in Fig. 7. As the path length increased, the positioning accuracy of CAMERA+IMU drifted significantly, where the positioning accuracy was the lowest among all positioning methods and the differences were sharp. LIDAR positioning also drifted but was not significant in a short time span, e.g., in a single trajectory.

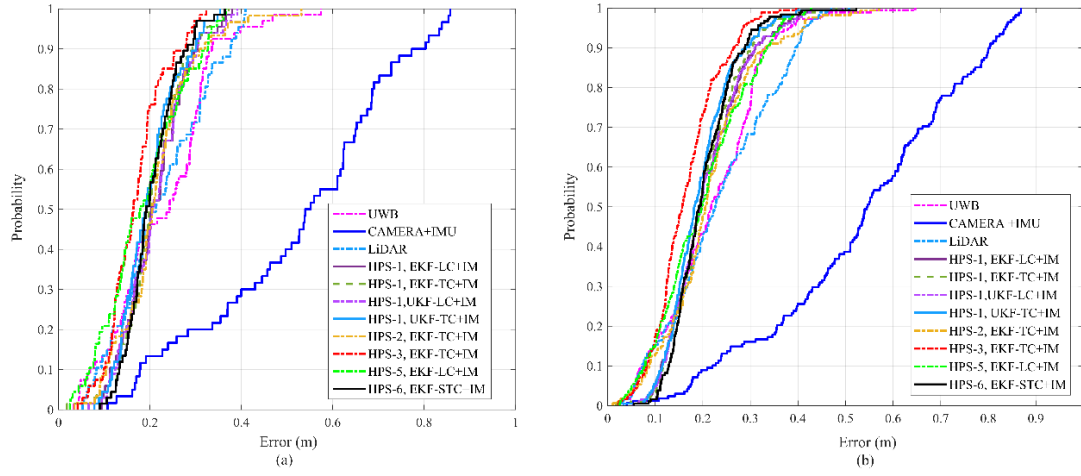


Fig. 6. The CDFs of different positioning methods in the Indoor I-1 (a) and Indoor I-3 (b).

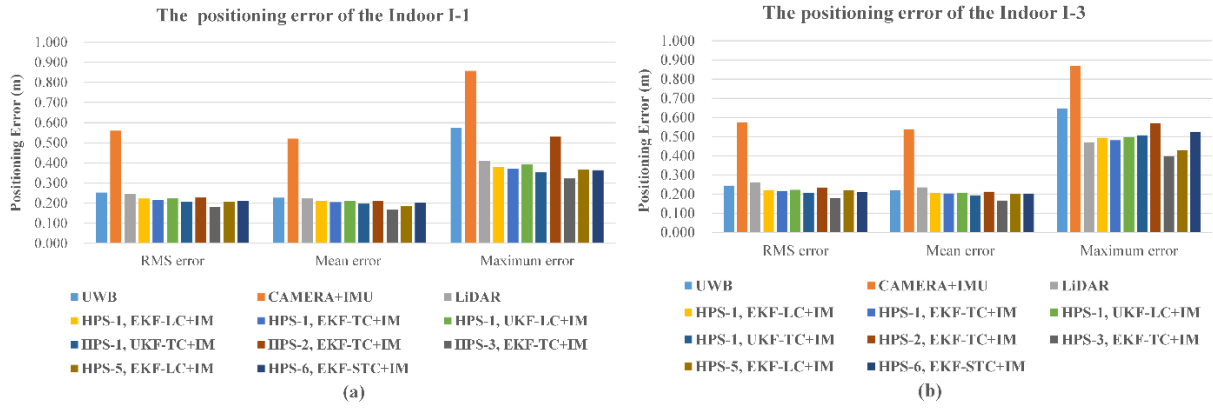


Fig. 7. The statistics of different positioning methods in the Indoor I-1 (a) and Indoor I-3 (b).

For Indoor-II, the CDFs and error statistics are illustrated in Fig. 8 and Fig. 9, respectively. As shown in Fig. 8, the six HPSs have higher positioning accuracy than that of the absolute positioning subsystem using UWB and the relative positioning subsystem using CAMERA+IMU, LiDAR, and RADAR. According to Fig. 9, the RMS, mean, and maximum errors of the six HPSs were all smaller than that of a single positioning system. In this test, the positioning error of RADAR and CAMERA+IMU was relatively large, and the positioning accuracy of LiDAR was almost the same as that of UWB and the HPS-3 (UWB+LiDAR). The maximum error of the HPS-4 (UWB+RADAR) was 0.531 m in Indoor II-1, and 0.605 m in Indoor II-3. fusing UWB and RADAR reduced 16.77% and 25.680% errors. The accuracy of the HPS-5 (IMU+CAMERA+LiDAR) was slightly higher than that of the UWB alone. The maximum, mean, and RMS errors of the HPS-6 (UWB+IMU+CAMERA+LiDAR) were 0.214 m, 0.070 m, and 0.080 m in Indoor II-3, respectively.

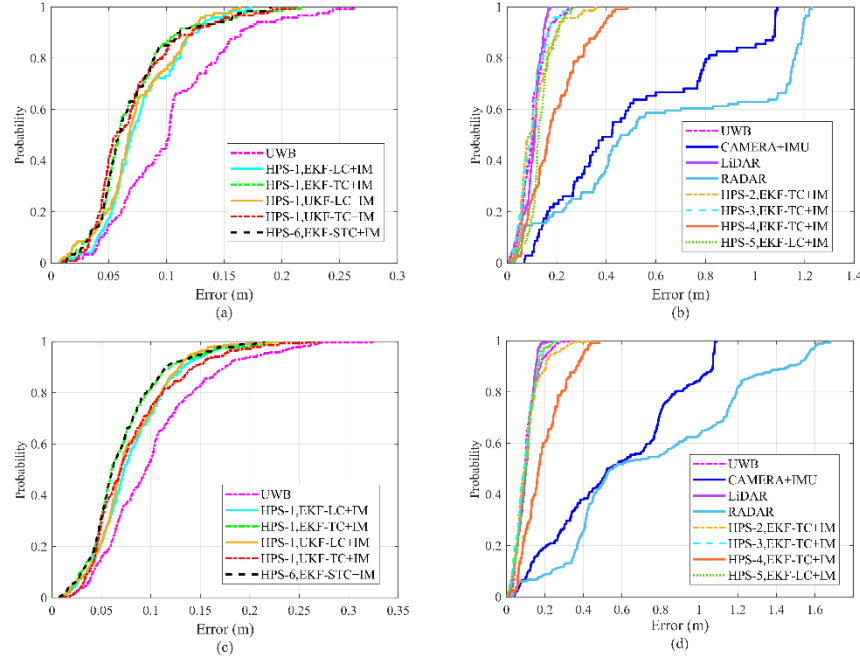


Fig. 8. The CDFs of different positioning methods in the Indoor II-1 (a, b) and Indoor II-3 (c, d).

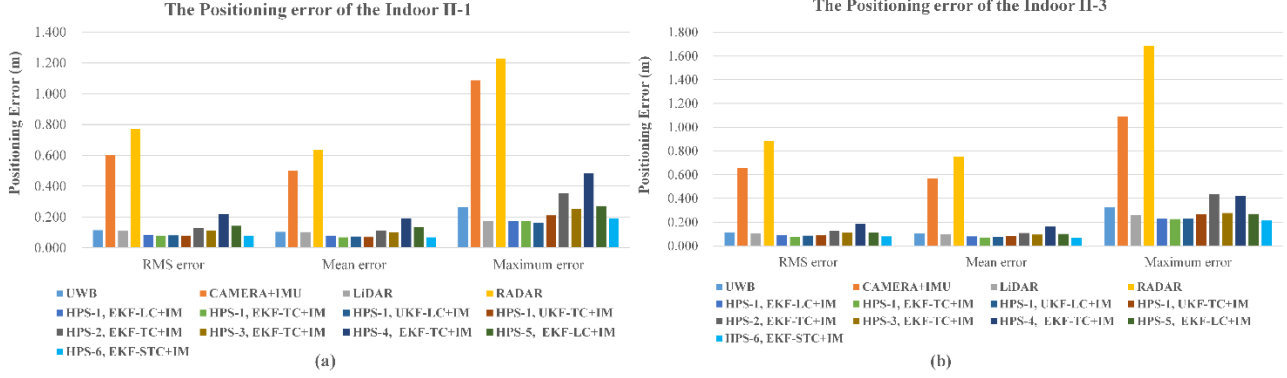


Fig. 9. The statistics of different positioning methods in the Indoor II-1 (a) and Indoor II-3 (b).

4.2 Outdoor Scenarios

The experimental results in an empty outdoor square and an empty basketball court are presented in this section. The outdoor-related experiments of the RADAR were only presented in basketball court (Outdoor-III) scenes to compare with experimental results of other positioning methods.

The CDFs of positioning error and error statistical values corresponding to the Outdoor I-1 and Outdoor I-3 are shown in Fig.10 and Fig. 11.

As shown in Fig. 10, the HPS-1 (UWB+IMU, UKF-TC+IM, EKF-TC+IM) outperformed all other positioning methods. The mean positioning errors of HPS-1 (UWB+IMU) using UKF-TC+IM and EKF-TC+IM were both around 0.090 m. The positioning means error of the HPS-2 (UWB+CAMERA+IMU) and the HPS-3 (UWB+LIDAR) were both around 0.180 m. In this experiment, the positioning error of the CAMERA+IMU was greater than that of the Indoor I scene due to the reason that the Outdoor-I scene had fewer texture features than the Indoor-I scene. However, the HPS-2 (UWB+ CAMERA+IMU) significantly improved the positioning in comparison with CAMERA+IMU, which showed that absolute positioning can significantly improve the relative position, especially when the relative positioning was unreliable. The HPS-5 (IMU+CAMERA+LIDAR) had the lowest positioning accuracy among different HPSs since the positioning accuracies of LIDAR and CAMERA was relatively low in Outdoor-I. The HPS-6

(UWB+IMU+CAMERA+LIDAR) improved the positioning accuracy in comparison with HPS-5 by adding the UWB positioning.

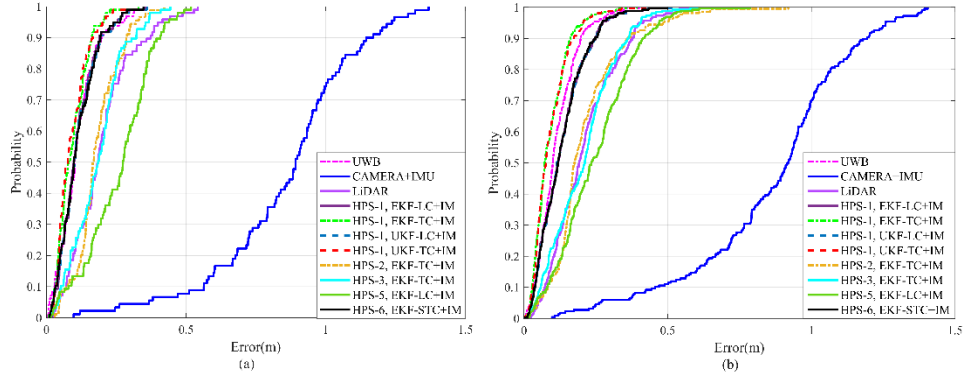


Fig. 10. The CDFs of different positioning methods in the Outdoor II-1 (a) and Outdoor II-3 (b).

As shown in Fig. 11, the mean positioning error of the UWB was 0.110 m. In HPS-1 (UWB+IMU), the TC had a slightly higher positioning accuracy than the LC, and the positioning accuracy of the LC was almost the same as the UWB positioning alone. These results showed that, without NLOS, UWB was accurate and the improvement of adding IMU to UWB was minor. The maximum, mean, and RMS errors of the HPS-1 (EKF-TC+IM, UKF-TC+IM) were around 0.400 m, 0.090 m, and 0.110 m, respectively. The HPS-1 had the smallest maximum error among all HPSs in Outdoor I-1, which was less than 0.370 m.

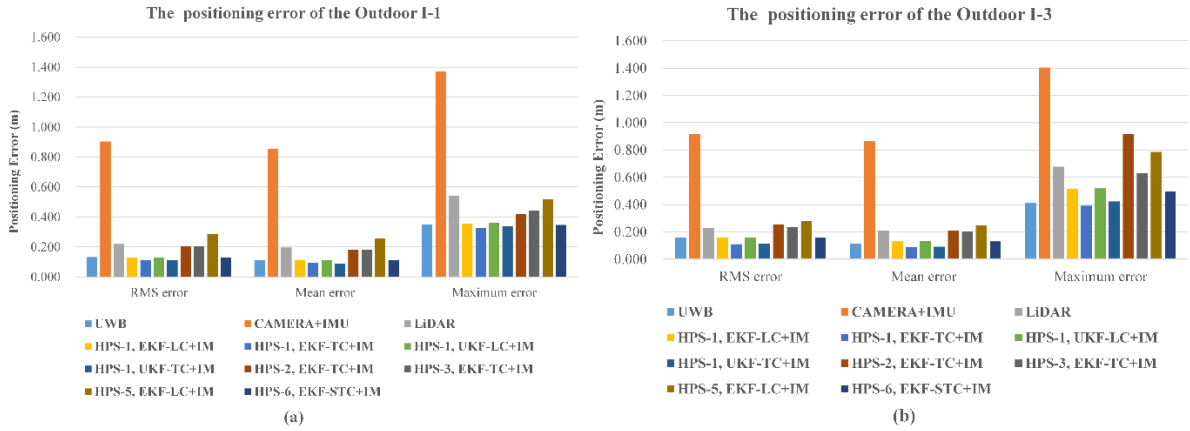


Fig. 11. The statistics of different positioning methods in the Outdoor I-1 (a) and Outdoor I-3 (b).

The CDFs of positioning error and error statistical values corresponding to the Outdoor II-1 and Outdoor II-3 are shown in Fig. 12 and Fig. 13 respectively.

According to Fig. 12, the positioning accuracies of the HPS-1, -3, -5, and -6 were nearly equal in the Outdoor II, e.g., the 90% positioning error of the HPS-1, -3, -5, and -6 were within 0.020 m. The proposed HPSs all improved the positioning accuracies of the relative positioning, and the improvement in the CAMERA+IMU accuracy was particularly significant. The UWB and LiDAR have almost the same positioning accuracy in this experiment. The positioning accuracies of the HPS-3 (mean error was 0.080 m) were higher than that of the HPS-3 in Outdoor II. The positioning accuracies of the HPS-5 (mean error was 0.090 m) in the Outdoor II were higher than that of HPS-5 in Outdoor II since the positioning accuracies of the LiDAR in the Outdoor II were higher.

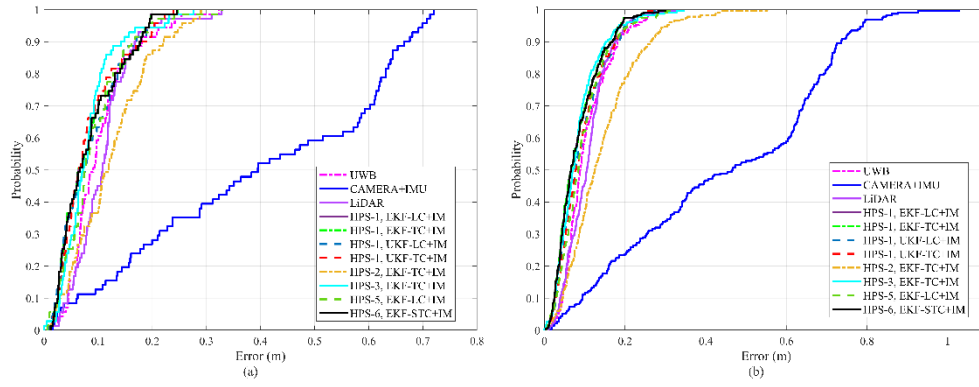


Fig. 12. The CDFs of different positioning methods in the Outdoor II-1 (a) and Outdoor II-3 (b).

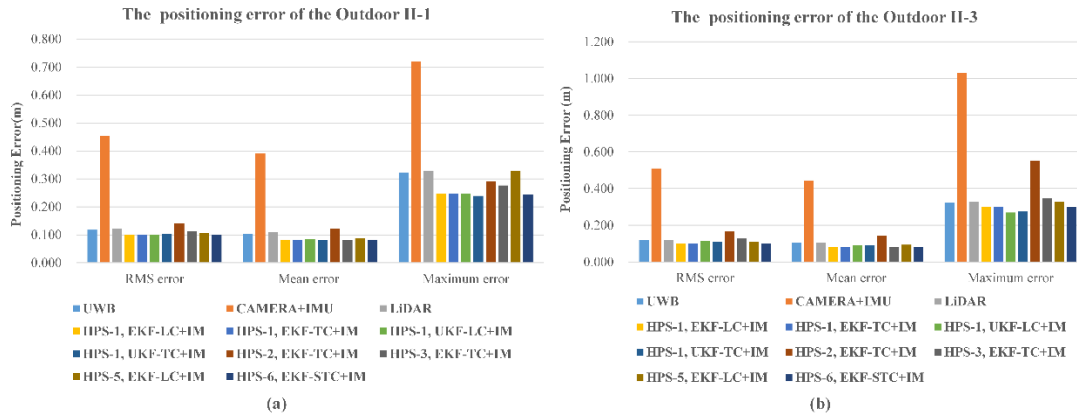


Fig. 13. The statistics of different positioning methods in the Outdoor II-1 (a) and Outdoor II-3 (b).

According to Fig. 13 (a) and (b), the maximum and mean positioning errors of the HPS-1 (UWB+IMU) were within 0.250 m and around 0.080 m in Outdoor II-1, respectively. The positioning accuracy of the four fusion algorithms of the HPS-1 was nearly equal in Outdoor II-1 and II-3. The maximum error of the CAMERA+IMU was 0.720 m and 1.028 m in the Outdoor II-1 and II-3, respectively. The maximum errors of the HPS-2 (UWB+CAMERA+IMU) were 0.290 m and 0.553 m in the Outdoor II-1 and II-3, respectively. The positioning accuracy of the HPS-3 (UWB+LiDAR) was slightly higher than that of the LiDAR in the Outdoor II-3. The mean and RMS errors of the HPS-5 (i.e., 0.094 m and 0.110 m) were slightly lower than that of the UWB (i.e., 0.104 m and 0.119 m) in this experiment. The HPS-6 (UWB + IMU + CAMERA+LiDAR) effectively achieved absolute positioning using the UWB and relative positioning based on IMU, CAMERA, and LiDAR. The mean and RMS errors of the proposed HPSs were almost the same in this experiment, which shows that in a simple scenario (without NLOS, and abundant visual textures), the positioning accuracies of all solutions were almost equally good.

5. Outcomes

Yao, H., Liang, X., Chen, R., Wang, X., Qi, H., Chen, L., Wang, Y., 2024. A Benchmark of Absolute and Relative Positioning Solutions in GNSS Denied Environments. *IEEE Internet of Things Journal* 11, 4243–4273. <https://doi.org/10.1109/IJOT.2023.3300018>.

Wang, X., Liang, X., Campos, M., Zhang, J., Wang, Y. 2024. Benchmarking of laser-based simultaneous localization and mapping methods in forest environments. *IEEE Transactions on Geoscience and Remote Sensing*, 62, 1-21. <https://doi.org/10.1109/TGRS.2024.3439438>.

Wang, X., Yao, H., Ma, Y., Liang, X. 2023. A Comparison Study of Low-Cost Personal Laser Scanning Systems for Forest Plot-Level Inventories. *The International Archives of the Photogrammetry, Remote Sensing and Spatial Information Sciences*, 48, 1809-1815. <https://doi.org/10.5194/isprs-archives-XLVIII-1-W2-2023-1809-2023>